Does the conductivity of interconnect coatings matter for solid oxide fuel cell applications?

(article starts on next page)

Does the conductivity of interconnect coatings matter for solid oxide fuel cell applications?

Claudia Goebel*, Alexander G. Fefekos, Jan-Erik Svensson, Jan Froitzheim

Chalmers University of Technology, Department of Chemistry and Chemical Engineering, Division of Energy and Materials, Kemivägen 10, 41296, Gothenburg, Sweden

HIGHLIGHTS

- Different Co coating thicknesses are exposed to air for 500 h at 600 °C.
- The coating thickness does not significantly affect the ASR.
- The contribution of the Co_3O_4 coating to the ASR is negligible.
- Theoretical calculations verify that the main contributor to the ASR is Cr_2O_3.
- The results can be generalized for most coating materials and temperatures.

ARTICLE INFO

ABSTRACT

The present work aims to quantify the influence of typical interconnect coatings used for solid oxide fuel cells (SOFC) on area specific resistance (ASR). To quantify the effect of the coating, the dependency of coating thickness on the ASR is examined on Crofer 22 APU at 600 °C. Three different Co coating thicknesses are investigated, 600 nm, 1500 nm, and 3000 nm. Except for the reference samples, the material is pre-oxidized prior to coating to mitigate the outward diffusion of iron and consequent formation of poorly conducting $(Co,Fe)_3O_4$ spinel. Exposures are carried out at 600 °C in stagnant laboratory air for 500 h and subsequent ASR measurements are performed. Additionally the microstructure is investigated with scanning electron microscopy (SEM). On all pre-oxidized samples, a homogenous dense Co_3O_4 top layer is observed beneath which a thin layer of Cr_2O_3 is present. As the ASR values range between 7 and 12 mΩcm^2 for all pre-oxidized samples, even though different Co_3O_4 thicknesses are observed, the results strongly suggest that for most applicable cases the impact of the coating on ASR is negligible and the main contributor is Cr_2O_3.

1. Introduction

Interconnects are an essential part of solid oxide fuel cells (SOFC), where they connect multiple cells to form a fuel cell stack, thus increasing the overall potential of a fuel cell [1]. Therefore, one important factor of any interconnect material is its electrical resistance at operating temperatures. In theory, the resistance should be negligible when using ferritic stainless steel interconnects, which is the norm today [1,2]. However, due to corrosion throughout the operation of a fuel cell, a continuously growing oxide layer occurs on the interconnect, resulting in an increase in resistivity. Issues such as Cr-evaporation and other corrosion-related problems can easily be decreased by applying coatings to the steel. In recent years, plenty of studies have been published on highly conductive coatings, which are thought to lower the area specific resistance (ASR) of the interconnect significantly even

after long-term operations [3–14]. The most prominent suggestions are compounds with spinel structure as these are easily deposited onto the steel. Besides applying the spinel coating directly to the steel by, for example, screen printing or physical vapor deposition (PVD), a different, more cost-efficient approach is to apply a metallic coating instead. The metal or metals will then oxidize to form M_3O_4 [15–17] during fuel cell operation. An extensive list of different spinel conductivities at 800 °C can be found in Ref. [18]. Especially $Cu_{1.3}Mn_{1.7}O_4$ and $MnCo_2O_4$ stand out with high conductivities, $\sigma < 225$ S cm^{-1} at 750 °C and $\sigma < 60$ S cm^{-1} at 800 °C, respectively. To increase conductivity even further, dopants such as Cu or Ni have been suggested as additives to the $(Co,Mn)_3O_4$ spinel [7,9]. However, the contribution of this coating to the overall ASR remains unknown. This is especially important as a continuously growing Cr_2O_3 layer is always present below the coating. With regard to the low conductivity of Cr_2O_3, which

Table 1
Composition of Crofer 22 APU in weight%.

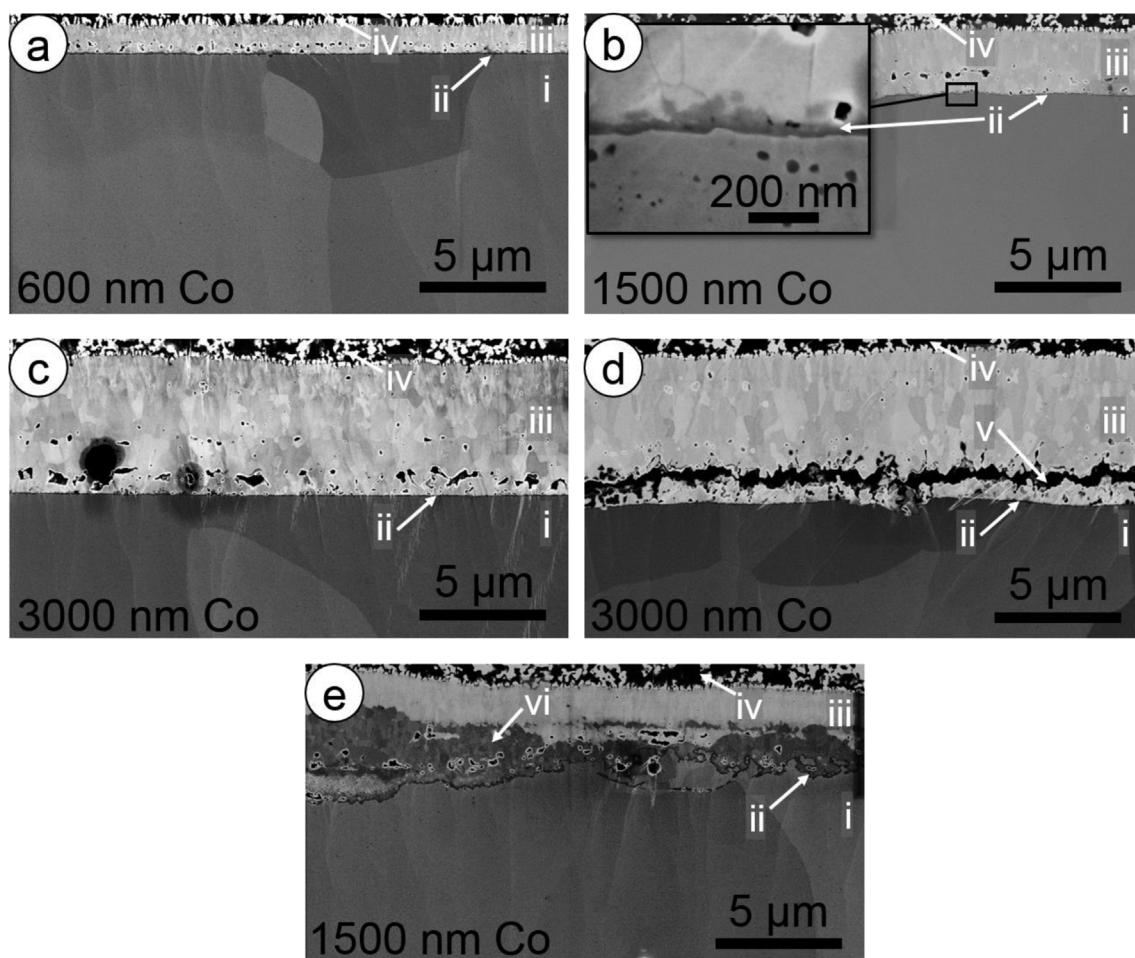| Crofer 22 APU	Fe	Cr	Mn	La	Ti	Al	Cu	Si	P	C	S
W.-Nr. 1.4760	Bal.	22.92	0.38	0.09	0.06	0.01	0.01	0.01	0.005	0.004	< 0.002

Fig. 1. SEM images of BIB milled cross-sections of Co coated Crofer 22 APU exposed for 500 h at 600 °C in stagnant, laboratory air. All samples were Co coated according to the following specifications a) a pre-oxidized sample with 600 nm Co coating, b) a pre-oxidized sample with 1500 nm Co coating, c) a pre-oxidized sample with 3000 nm Co coating, d) a pre-oxidized sample with 3000 nm Co coating, which showed signs of spallation after exposure, and e) a non-pre-oxidized sample with 1500 nm Co coating. All phases were identified as follows: i) steel, ii) thin Cr_2O_3 layer, iii) Co_3O_4, iv) Pt electrode, v) spallation crack, and vi) $(Co,Cr,Fe)_3O_4$.

ranges between 0.001 and 0.05 S cm^{-1} [19–26], the main contributor to the overall ASR is expected to be Cr_2O_3 in most practical cases.

To investigate the contribution of all oxides to the overall ASR, the moderately conductive Co_3O_4 (σ = 6.7 S cm^{-1} at 800 °C [18]) coating was applied to Crofer 22 APU with different thicknesses and, subsequently, exposed at 600 °C. For well adherent and dense coatings, it can be assumed that, if the coating significantly affects the ASR, thicker coatings will result in higher ASR values. Therefore a metallic Co conversion coating was prepared on Crofer 22 APU with three different Co coating thicknesses, 600 nm, 1500 nm, and 3000 nm, and the ASR was measured after 500 h of exposure in stagnant laboratory air at 600 °C. This temperature is typical for the lower end of SOFC operating conditions and is expected to result in a very thin Cr_2O_3 layer, and, thus, any effect of the Co coating thickness on the ASR can be expected to be the most pronounced.

2. Materials and methods

For this study, 15 × 15 × 0.3 mm^3 large coupons of Crofer 22 APU

were used. The composition of this material is shown in Table 1. The as-received and cut-out samples were ultrasonically cleaned in acetone and ethanol. Except for the reference case, all samples were pre-oxidized for 3 min at 900 °C in air prior to coating. Coatings were applied by Sandvik Materials Technology using PVD. Chosen Co coating thicknesses were 600 nm, 1500 nm, and 3000 nm. After coating, all samples were again ultrasonically cleaned in acetone and ethanol and, subsequently, exposed for 500 h at 600 °C in stagnant laboratory air.

After exposure, ASR measurements were performed by sputtering a defined area of 1 cm^2 with a thin Pt layer, followed by painting with the Pt paste Metalor 6926. Sintering of the Pt paint was achieved in a two-step process, a drying step for 10 min at 150 °C and a sintering step for 1 h at 600 °C. The ASR values were then measured according to the 4-point probe method in DC mode using the NorECs Probostat (Norway) and a Keithley 2400 source meter. The applied current was set to 100 mA cm^{-2}, and the ASR values were measured directly at exposure temperature, as well as during the cooling down phase, to verify semi-conductive behavior. More details on the ASR measurements can be found in Refs. [27] and [28]. Cross-sections were prepared using a Leica
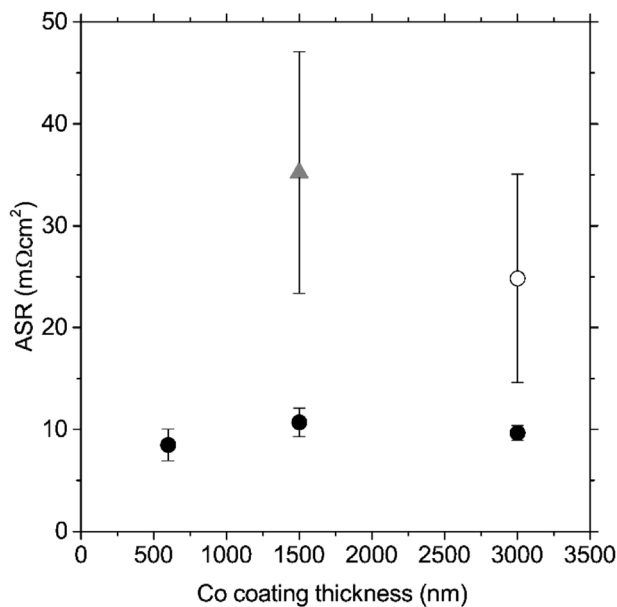
Fig. 2. Ex-situ recorded ASR values for Co coated Crofer 22 APU exposed for 500 h at 600 °C in stagnant laboratory air. Samples were coated with different Co coating thicknesses, 600 nm, 1500 nm, and 3000 nm Co. Circles correspond to samples that were pre-oxidized prior to Co coating; whereas samples depicted as triangles were not pre-oxidized prior to Co coating. Empty symbols indicate samples that showed signs of spallation. Errorbars indicate standard deviations.

Table 2
Literature values and calculated values for the conductivity and corresponding resistivity of Co_3O_4 and Cr_2O_3. Ea and $\sigma_{800°C}$ correspond to literature values, $\sigma_{600°C}$ is calculated using Equation (3), L represents the thickness of the observed oxide layer obtained from the cross-sections, and $R_{600°C}$ is calculated according to Equation (2) with the area A = 1 cm^2.

	E_a (eV)	$\sigma_{800°C}$ (S·cm^{-1})	$\sigma_{600°C}$ (S·cm^{-1})	L (nm)	$R_{600°C}$ (mΩ)
Co_3O_4	0.79 [32]	6.7 [18]	0.9462	1200	0.13
				5700	0.60
Cr_2O_3	0.46 [23]	0.008 [23]	0.0026	40	1.56

TIC3X Broad Ion Beam (BIB) mill. The resulting cross-sections were analyzed with an Ultra 55 FEG Scanning Electron Microscope (SEM) equipped with an Oxford Inca Energy Dispersive X-ray (EDX) system. To support the SEM/EDX results X-ray diffraction (XRD) measurements were performed using a Siemens D5000 diffractometer with Cu-K$_\alpha$ radiation.

3. Results

Fig. 1a, b, and c show SEM micrographs of pre-oxidized Co coated Crofer 22 APU (600 nm, 1500 nm and 3000 nm), which were exposed for 500 h at 600 °C in stagnant laboratory air. The different Co coating thicknesses, 600 nm, 1500 nm, and 3000 nm, resulted in roughly 1.2 μm, 2.8 μm, and 5.7 μm thick Co_3O_4, respectively. The volume increase is in accordance with the Pilling-Bedworth ratio of 1.98 [29] for Co_3O_4. EDX analysis confirmed that a nearly pure Co_3O_4 layer had formed, with very low and only localized incorporation of Mn (below 0.2 atomic%), Fe (below 0.9 atomic%) and Cr (below 0.9 atomic%). The Co_3O_4 layer was homogenous for all three cases, and its thickness hardly varied over each sample surface. The presence of Co_3O_4 was confirmed by XRD (data not shown). The thermally grown Cr_2O_3, located below the Co_3O_4 layer can be clearly seen in the inset in Fig. 1b, and was similarly thin, 35–45 nm, for all pre-oxidized samples.

Fig. 1d depicts an exposed pre-oxidized 3000 nm Co coated sample that showed spallation of the coating after the sample was removed

from the furnace. This delamination is clearly visible in the SEM image (Fig. 1d), which shows a spallation crack in the Co_3O_4 layer.

Fig. 1e visualizes a reference sample, which was not pre-oxidized prior to coating; instead a 1500 nm thick coating was applied directly to the as-received material. A thinner Co_3O_4 layer, compared to the corresponding pre-oxidized sample in Fig. 1b, was observed and, even more important, a thick and irregular $(Co,Cr,Fe)_3O_4$ spinel layer had formed. A thin Cr_2O_3 layer was present beneath the $(Co,Cr,Fe)_3O_4$ spinel. Similar results for samples of non-pre-oxidized ferritic stainless steels have been published by *Falk-Windisch* et al. [28,30], who have shown that, at intermediate temperature, the metal/metal contact between steel and a metallic coating results in interdiffusion and increased oxide scale growth. This would prohibit the identification of the contribution of the coating to the ASR and, for this reason, pre-oxidized steel was used in this study.

Recorded ASR values are depicted in Fig. 2. Black symbols correspond to pre-oxidized samples with the different Co coating thicknesses, 600 nm, 1500 nm, and 3000 nm. Some of the 3000 nm Co coated samples showed signs of spallation, these values are depicted as empty symbols. The reference ASR values from samples that were not pre-oxidized prior to applying the 1500 nm thick Co coating are shown as grey triangles.

The ASR values of all pre-oxidized non-spalled samples (black symbols) ranged between 7 and 12 mΩcm^2. A very slight trend towards higher ASR values with increasing Co coating thickness is observable. However, this trend was also well inside the spread of each measurement. The spalled samples with a 3000 nm thick Co coating exhibited higher ASR values, between 16 and 37 mΩcm^2, compared to the non-spalled samples. A larger spread in ASR values was observed for these samples. Similarly non-pre-oxidized samples also showed much higher ASR values with a large spread between 23 and 50 mΩcm^2.

4. Discussion

Even though major differences in the thickness of the Co_3O_4 layer can be seen in the SEM micrographs of all pre-oxidized, non-spalled samples, the ASR values hardly differed, which suggests that the ASR is not dependent on the Co coating thickness, and the main contributor to the overall resistance is the thermally grown Cr_2O_3. This interpretation is further strengthened by estimating the theoretical contribution of each oxide to the overall ASR value based on literature values for the respective conductivities and layer thicknesses. Certain limitations must be considered when literature values are used. The literature values are subject to a large spread and have been obtained for pure, dense bulk samples, which is not necessarily the case for a thermally grown oxide. Especially incorporation of Fe into the Cr_2O_3 scale, which is often seen in thermally grown oxides, can greatly increase the conductivity of this scale. The oxide scale is also subject to a steep oxygen activity gradient, which, in turn, is expected to affect the defect structure in the oxide.

For the theoretical calculations, the oxides can be considered in-series connected resistors and, with the resistance of each oxide given by Equation (1), the resulting overall ASR is given by equation (2).

$$R = \frac{1}{\sigma} \cdot \frac{L}{A} \tag{1}$$

$$ASR = A \cdot R_{tot} = A \cdot \left(R_{Cr_2O_3} + R_{Co_3O_4} \right) = A \cdot \frac{1}{A} \left(\frac{L_{Cr_2O_3}}{\sigma_{Cr_2O_3}} + \frac{L_{Co_3O_4}}{\sigma_{Co_3O_4}} \right) \tag{2}$$

where R is the resistance, σ the conductivity, and L the thickness of the oxide and A is the measured area. The literature values for the experimentally observed conductivities were measured at 800 °C; whereas the experimentally observed ASR values in this study were recorded at 600 °C. For this reason, the conductivities must be converted using their respective activation energies. These two values relate to each other according to Equation (3).

$$\sigma = \sigma_0 \cdot e^{\frac{-E_a}{R \cdot T}} \qquad (3)$$

where σ_0 is a pre-exponential factor, E_a is the activation energy, R is the ideal gas constant and T the absolute temperature. The literature values used for all calculations along with the resulting conductivities and resistivities are summarized in Table 2. Similar to the reported conductivity for Cr_2O_3 also the literature values for the activation energy of Cr_2O_3 are subject to a large spread and values between 0.25 and 0.82 eV (various measurements below 850 °C [20–26]) have been reported. In this work, the observed conductivity and respective activation energy of *Park* et al. [23] were used for all theoretical calculations. These values were chosen, because they are very similar to the average values that have been found over many different publications [19–26,31]. Discussions on and comparisons of the Cr_2O_3 conductivity can be found elsewhere [28,31]. For Co_3O_4 the reported activation energy of Tareen et al. [32] was used, E_a (Co_3O_4) = 0.79 eV (measured below 650 °C).

The results of the theoretical calculations showed that, in the case of $L(Co_3O_4)$ = 1.2 μm ($\triangleq$ 600 nm Co coating), the contribution of Cr_2O_3 to the overall ASR can be expected to be larger than the contribution of the cobalt oxide by a factor of 10. This relation, although slightly less prominent, also stays true when $L(Co_3O_4)$ = 5.7 μm is assumed, which corresponds to a 3000 nm thick Co coating and results in a resistance of $R(Co_3O_4)$ = 0.60 mΩ. The contribution of both oxides to the overall ASR was found to be well represented by the theoretical calculations, and the insignificance of the conductivity of the coating layer was further verified.

The ASR values of the spalled samples of the 3000 nm thick Co coating were higher than the values of the corresponding non-spalled samples (Fig. 2). This can be easily explained by comparing the SEM micrographs for both cases (Fig. 1c and d). A spallation gap was observed in all spalled samples, but was not present in the non-spalled samples. This gap (Fig. 1d) can easily lead to higher ASR values due to contact issues during measurement. The spread in ASR values can also be explained by the spallation that occurred, to different extents, on the spalled samples.

Relatively high ASR values were also measured for the reference sample (Fig. 2). In combination with the SEM micrograph in Fig. 1e, it is obvious that the mixed $(Co,Fe)_3O_4$ also contributed to the overall ASR value of the sample. This was not unexpected as the conductivity of $CoFe_2O_4$ (σ = 0.93 S cm^{-1} at 800 °C [18]) is much lower than that of Co_3O_4 and closer to the conductivity of Cr_2O_3. The SEM image indicates that the spinel composition was not homogeneous across the whole layer, and this indicates that doping of Cr might be present. This could lead to a further reduction in the conductivity of this layer. The high deviation in ASR values can probably be contributed to the fact that the mixed spinel layer was not very homogeneous and exhibited a major difference in thickness throughout the sample.

Results indicate that the Co coating layer did not contribute significantly to the overall resistance. The low exposure temperature of 600 °C resulted in a very thin Cr_2O_3 scale (L = 40 nm); at higher operating temperatures, the Cr_2O_3 would be thicker, and the contribution of Cr_2O_3 would be even more dominant. At 800 °C Cr_2O_3 scales of approximately 1 μm are typical for a Crofer 22 APU type material after 1000 h of exposure. Under these conditions, considering the data in Table 2, the contribution of Cr_2O_3 will exceed that of Co_3O_4 unless the coating is thicker than 80 μm. For this reason and because Co_3O_4 is only moderately conductive compared to other typical interconnect coatings, such as the aforementioned $Cu_{1.3}Mn_{1.7}O_4$ and $MnCo_2O_4$, it can be concluded that the coating conductivity is negligible for the overall ASR, with the exception of thick (> 5 μm) coatings, low temperatures, and/or coatings with a lower conductivity than Co_3O_4.

5. Conclusion

After 500 h exposure in stagnant laboratory air, pre-oxidized Crofer 22 APU with Co coating thicknesses ranging from 600 nm to 3000 nm

showed very low ASR values between 7 and 12 mΩcm^2. These low ASR values in combination with the corresponding SEM micrographs for the non-spalled pre-oxidized materials clearly show that the main contributor to the ASR values was the Cr_2O_3 layer, and no observable contribution of the Co_3O_4 layer to the ASR was visible after 500 h exposures at 600 °C. These findings match the simple theoretical calculations well, which show that the main contributor to the overall ASR is the Cr_2O_3 layer (a factor of 10 higher resistance than Co_3O_4 for a 600 nm thick metallic Co coating). It was found that highly conductive coatings are not the solution to the high resistivity issues that may arise during fuel cell operation. Instead the aim should be to focus on effectively limiting the growth of very low conductive layers, such as Cr_2O_3, as well as ensuring good electrode/interconnect contact.

References

[1] J.W. Fergus, Mater. Sci. Eng. A 397 (2005) 271–283 https://doi.org/10.1016/j.msea.2005.02.047.

[2] W.Z. Zhu, S.C. Deevi, Mater. Res. Bull. 38 (2003) 957–972 https://doi.org/10.1016/S0025-5408(03)00076-X.

[3] G. Chen, X. Xin, T. Luo, L. Liu, Y. Zhou, C. Yuan, C. Lin, Z. Zhan, S. Wang, J. Power Sources 278 (2015) 230–234 https://doi.org/10.1016/j.jpowsour.2014.12.070.

[4] V. Miguel-Pérez, A. Martínez-Amesti, M.L. Nó, A. Larrañaga, M.I. Arriortua, J. Power Sources 243 (2013) 419–430 https://doi.org/10.1016/j.jpowsour.2013.05.109.

[5] S. Chevalier, G. Caboche, K. Przybylski, T. Brylewski, J. Appl. Electrochem. 39 (2009) 529–534 https://doi.org/10.1007/s10800-008-9726-9.

[6] T. Brylewski, A. Kruk, M. Bobruk, A. Adamczyk, J. Partyka, P. Rutkowski, J. Power Sources 333 (2016) 145–155 https://doi.org/10.1016/j.jpowsour.2016.09.136.

[7] Y. Xu, Z. Wen, S. Wang, T. Wen, Solid State Ionics 192 (2011) 561–564 https://doi.org/10.1016/j.ssi.2010.05.052.

[8] N. Shaigan, W. Qu, D.G. Ivey, W. Chen, J. Power Sources 195 (2010) 1529–1542 https://doi.org/10.1016/j.jpowsour.2009.09.069.

[9] B.-K. Park, J.-W. Lee, S.-B. Lee, T.-H. Lim, S.-J. Park, C.-O. Park, R.-H. Song, Int. J. Hydrogen Energy 38 (2013) 12043–12050 https://doi.org/10.1016/j.ijhydene.2013.07.025.

[10] B. Talic, S. Molin, K. Wiik, P.V. Hendriksen, H.L. Lein, J. Power Sources 372 (2017) 145–156 https://doi.org/10.1016/j.jpowsour.2017.10.060.

[11] K. Lee, B. Yoon, J. Kang, S. Lee, J. Bae, Int. J. Hydrogen Energy 42 (2017) 29511–29517 https://doi.org/10.1016/j.ijhydene.2017.10.017.

[12] S.N. Hosseini, M.H. Enayati, F. Karimzadeh, A.M. Dayaghi, Metall. Mater. Trans. A 48 (2017) 3490–3496 https://doi.org/10.1007/s11661-017-4084-z.

[13] F. Shen, K. Lu, ACS Appl. Mater. Interfaces 9 (2017) 6022–6029 https://doi.org/10.1021/acsami.6b14562.

[14] K. Lee, B. Yoon, J. Kang, S. Lee, J. Bae, Int. J. Hydrogen Energy 42 (2017) 29511–29517 https://doi.org/10.1016/j.ijhydene.2017.10.017.

[15] J.G. Grolig, J. Froitzheim, J.-E. Svensson, J. Power Sources 248 (2014) 1007–1013 https://doi.org/10.1016/j.jpowsour.2013.08.089.

[16] M. Stanislowski, J. Froitzheim, L. Niewolak, W.J. Quadakkers, K. Hilpert, T. Markus, L. Singheiser, J. Power Sources 164 (2007) 578–589 https://doi.org/10.1016/j.jpowsour.2006.08.013.

[17] Y. Zeng, J. Wu, A.P. Baker, X. Liu, Int. J. Hydrogen Energy 39 (2014) 16061–16066 https://doi.org/10.1016/j.ijhydene.2013.11.101.

[18] A. Petric, H. Ling, J. Am. Ceram. Soc. 90 (2007) 1515–1520 https://doi.org/10.1111/j.1551-2916.2007.01522.x.

[19] P. Huczkowski, N. Christiansen, V. Shemet, L. Niewolak, J. Piron-Abellan, L. Singheiser, W.J. Quadakkers, Fuel Cell. 6 (2006) 93–99 https://doi.org/10.1002/fuce.200500110.

[20] J.A. Crawford, R.W. Vest, J. Appl. Phys. 35 (1964) 2413–2418 https://doi.org/10.1063/1.1702871.

[21] W.C. Hagel, A.U. Seybolt, J. Electrochem. Soc. 108 (1961) 1146–1152 https://doi.org/10.1149/1.2427973.

[22] H. Nagai, T. Fujikawa, K.-i. Shoji, Trans. Jpn. Ins. Met. 24 (1983) 581–588 https://doi.org/10.2320/matertrans1960.24.581.

[23] J.H. Park, K. Natesan, Oxid. Metals 33 (1990) 31–54 https://doi.org/10.1007/BF00665668.

[24] A. Holt, P. Kofstad, Solid State Ionics 69 (1994) 127–136 https://doi.org/10.1016/0167-2738(94)90401-4.

[25] Y. Larring, R. Haugsrud, T. Norby, J. Electrochem. Soc. 150 (2003) B374–B379 https://doi.org/10.1149/1.1587726.

[26] K. Huang, P.Y. Hou, J.B. Goodenough, Solid State Ionics 129 (2000) 237–250 https://doi.org/10.1016/S0167-2738(99)00329-X.

[27] J.G. Grolig, J. Froitzheim, J.-E. Svensson, J. Power Sources 284 (2015) 321–327 https://doi.org/10.1016/j.jpowsour.2015.03.029.

[28] H. Falk-Windisch, J. Claquesin, M. Sattari, J.-E. Svensson, J. Froitzheim, J. Power Sources 343 (2017) 1–10 https://doi.org/10.1016/j.jpowsour.2017.01.045.

[29] E. McCafferty, Introduction to Corrosion Science, Springer New York, 2010, p. 236.

[30] H. Falk-Windisch, J. Claquesin, J.-E. Svensson, J. Froitzheim, Oxid. Metals 89 (2018) 233–250 https://doi.org/10.1007/s11085-017-9782-9.

[31] J.G. Grolig, Coated Ferritic Stainless Steels as Interconnects in Solid Oxide Fuel Cells, Doctor of Philosophy Chalmers University of Technology, Gothenburg, Sweden, 2015, pp. 147–163.

[32] J.A.K. Tareen, A. Małecki, J.P. Doumerc, J.C. Launay, P. Dordor, M. Pouchard, P. Hagenmuller, Mater. Res. Bull. 19 (1984) 989–997 https://doi.org/10.1016/0025-5408(84)90212-90215.